The precipitation efficiency in subtropical region revealed by dual-polarimetric radar: TiMREX case study

Wei-Yu Chang[1,2,3] Jothiram Vivekanandan[2,3] Wen-Chau Lee[2,3]

Advanced Study Program(ASP)[1]
Earth Observing Laboratory(EOL)[2] / National Center for Atmospheric Research (NCAR)[3]

1. Introduction

The microphysical processes play an key role in the weather system. The net heating profile within the precipitation modulates thermodynamic fields, namely temperature and pressure, and further the kinematic fields. Despite the fact that the importance of microphysical process, the observation data is limited due the difficulty of acquiring such information, except remote-sensing data (e.g. dual-polarimetric radar).

One of numerous parameters of microphysical process: precipitation efficiency(PE), is used to characterize precipitation system. By studying PE, the water budget within the precipitation system could be understood. The multi-scale interaction of precipitation processes can be investigated as well and further applied to globe water circulation study. Moreover, understanding those factors associated with PE can be used for nowcasting and other further application (e.g. hydrology).

Several key scientific questions are:

✓PE in different precipitation process: convective & stratiform system?

✓PE in different precipitation system: frontal-precipitation system, deep convection, terrain influenced precipitation, marine and continental type precipitation?

✓PE in different microphysical processes: warm and cold rain processes?

✓PE at different developing stage (e.g. initiation, mature and dissipation stage)?

✓PE and corresponding drop size distribution?

In this following research, one squall line observed in subtropical region during TiMREX field project on June 14, 2008 is investigated in terms of its kinematic, microphysical field and precipitation efficiency (PE). The squall line approached Taiwan on early morning of June 14 accompanied with several rainbands (Fig. 1).

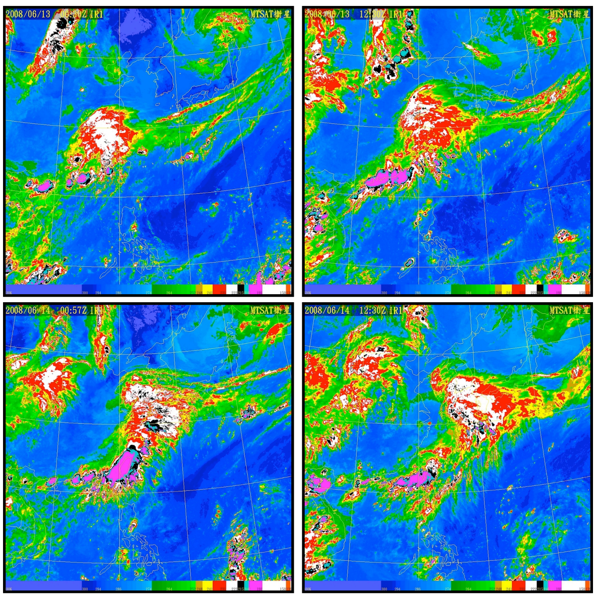

Fig. 1: IR satellite image from Jun. 13th 00 UTC to Jun. 14th 12 UTC.

The result from two convective precipitation systems associated with wide spread stratiform systems from 0930 ~ 1030 UTC (case 1) and 2100 ~ 2200 UTC (case 2) will be demonstrated. In this research, the PE for convective and stratiform precipitation system will be studied, as well as the kinematic and microphysical fields.

Three hourly sounding network (Fig. 2) and NCAR SPOL radar in southern Taiwan provide environmental moisture field, mesoscale dynamic and microphysical observation.

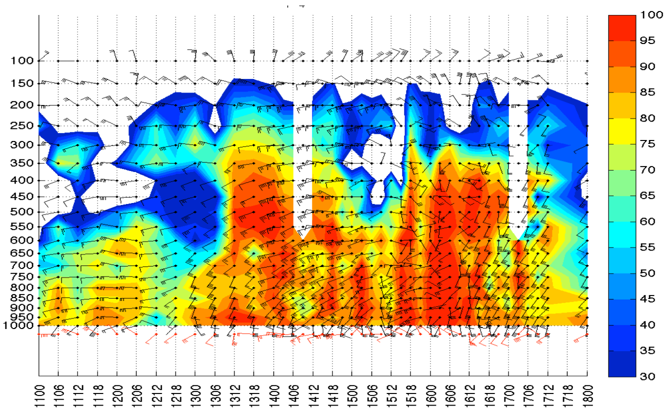

Fig. 2: Relative humidity field from Magong sounding station.

2. Algorithm and Data

The vertical integrated water vapor (q_v) and cloud (C) budgets can be expressed as (Sui et al. 2005),

$$\partial[q_v]/\partial t = [CONV_{qc}] + E_s - [\, S_{qv} \,],$$
$$\partial[C]/\partial t = [CONV_C] - P_s + [S_c],$$
$$[\, F \,] = \int \rho_{air} F dz$$

E_s = surface evaporation,

P_s = surface rainfall rate

$C = q_c + q_r + q_i + q_s + q_g$: total mixing ratio of could, rain, ice, snow and graupel

$S_{qv} = SI_{qv}(sink) - SO_{qv}(source)$

$SI_{qv}(sink) = [P_{CND}] + [P_{DEP}] + [P_{SDEP}] + [P_{GDEP}]$: Sink term of water vapor via condensation, deposition of ice, snow and graupel.

$SO_{qv}(source) = [P_{REVP}] + [P_{MLTG}] + [P_{MLTS}]$: Source term of water vapor via evaporation of rain, melting of graupel and snow.

$[S_C] = [S_{qv}] = \partial[C]/\partial t - [CONV_C] + P_s$

Two precipitation efficiencies are defined, (1) Large scale Precipitation efficiency (LSPE) and (2) Cloud Microphysical Precipitation efficiency (CMPE).

$$LSPE \equiv P_s / ([CONV_{qv}] + q_{v\ flux\_suf})$$

$$CMPE \equiv P_s / [S_C]$$

Therefore, the P_S is calculated from NCAR SPOL and the moisture field is estimated by using three hourly sounding data. The dual-synthesis adjusted wind field is derived from variational-based algorithm (Liou et al. 2009) with continuity and vorticity conservation constrain from SPOL, RCCG and RCKT radar in souther Taiwan (with 7.5 minutes time resolution). The liquid content (g/m^3) of rain, snow, ice and graupel are estimated by first applying particle identification (Vivekanandan et al. 1999) and calculated via constrain-DSD retrieval (Vivekanandan et al. 2004) and Z-M_{ice} relation (Carey et al. 2000).

$$M_{ice}\,(gkg^{-1}) = 1000\pi(\rho_i/\rho_a)N_0^{3/7}(5.28\times10^{-18}Z_H^{ice} / 720)^{4/7}$$

All of the calculations were performed between 2.0 and 15.0 km MSL due to the low level clutter contamination and the limitation of scanning strategy. Moreover, it can be noticed that the evaporation at surface and cloud water content is neglected due to the observation data.

3. Kinematic field

The squall line orients northeast to southwest direction and moves easterly (Fig. 3). As shown in Fig. 4, the individual convective systems move north-eastward with advection speed about 16 m/sec for case 1.

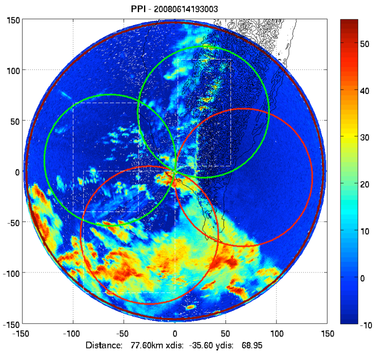

Fig. 3: The PPI plot of Z_{HH} measurement from NCAR SPOL at 0930 UTC.

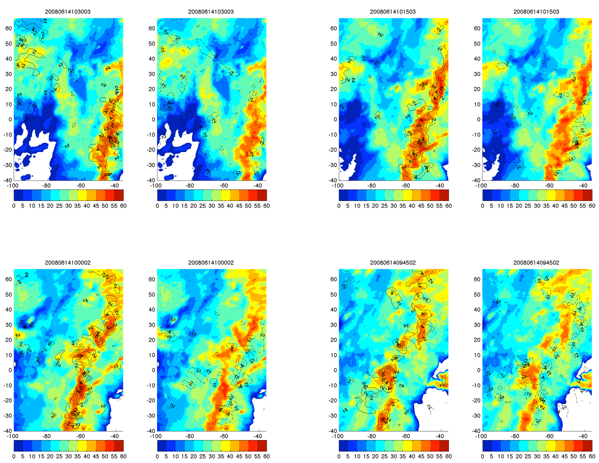

Fig. 4: The Z_{HH} at 2 km MSL with vertical volume maximum updraft and downdraft for 0945UTC, 1000UTC,1015UTC and 1030 UTC.

It can be seen that the maximum values of updraft and downdraft are about 10.0 and 8.0 m/sec, respectively. Moreover, the maximum downdrafts locate in the downstream of the rainband. Detail study will be performed in cross-section analysis.

The case 2 has east-west orientated convective system (Fig. 5) and move northward with advection speed about 7.0 m/sec (Fig. 6). Examining the vertical velocity field shows that the maximum value of updraft is about 8 m/sec, slightly lower compared to pervious case. Furthermore, there is no comparable strong downdraft compared to case 1. Also, case 2 has less organized system compared to case 1.

As shown in Fig 7, the vertical cross-section for case 1 indicates that the maximum updrafts locate at about 6.5 km MSL. The updraft lift raindrop above freezing level (5.0 km) and up to 6.0 km. The rear to front flow is about 2 m/sec at mid-level.

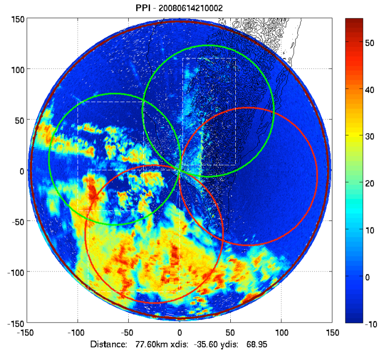

Fig. 5: The PPI plot of Z_{HH} measurement from NCAR SPOL at 2100 UTC.

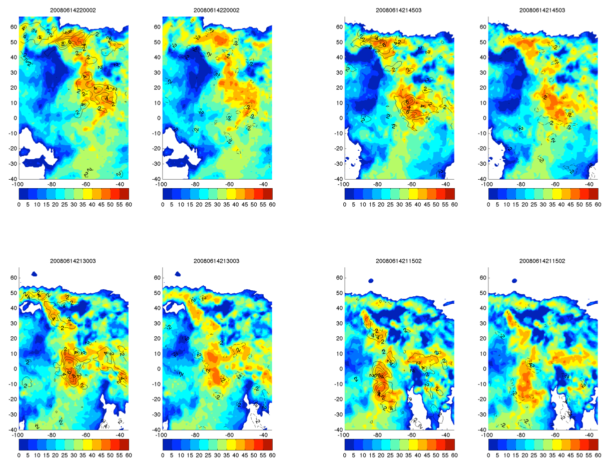

Fig. 6: The Z_{HH} at 2 km MSL with vertical volume maximum updraft and downdraft for 2115UTC, 2130UTC,2145UTC and 2200 UTC.

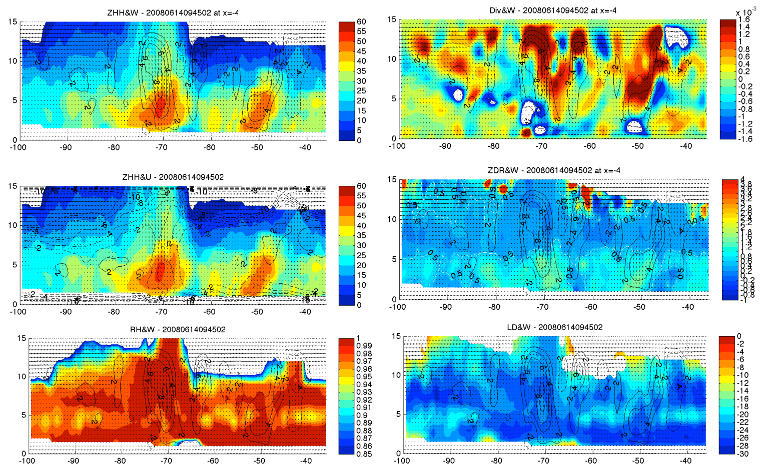

Fig. 7: The cross-section plot of Z_{HH}, divergence field, Z_{DR}, LDR and RH for case 1. The horizontal and vertical velocity are shown in contour lines.

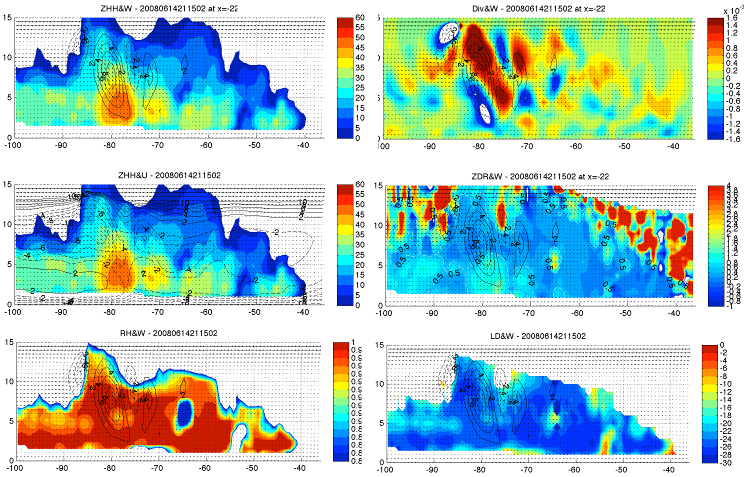

Fig. 8: Same as Fig. 7, but for case 2.

The Bright-band signature can be found most of place. The graupel signature can be seen at -70 km away from radar and 5 km above MSL as well. For case 2 (Fig. 8), the upstream tilted updraft and divergence field associate with a 4 m/sec downdraft at downstream region. The downstream shallow convection without bright-band signature indicates warm-rain process.

4.Microphysical field

The Contoured Frequency Altitude Diagram (CFAD) of NCAR SPOL measurements and retrieved rainfall rate and water content of two cases are studied. The CFADs are obtained for each case and divided into convective and stratiform region. The algorithm from Steiner et al. (1995) is applied to classify convective and stratiform precipitation. The examination of vertical cross-section of polarimetric measurements for convective and stratiform classification shows that the classification is sufficient for the PE study.

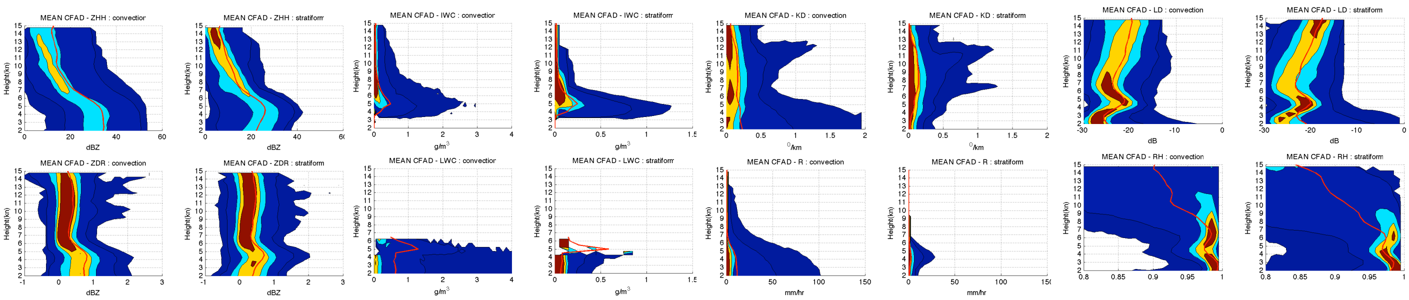

Fig. 9: The CFAD of Z_{HH}, Z_{DR}, LWC, IWC, KD, rianfall rate, LDR and RH for case 1.

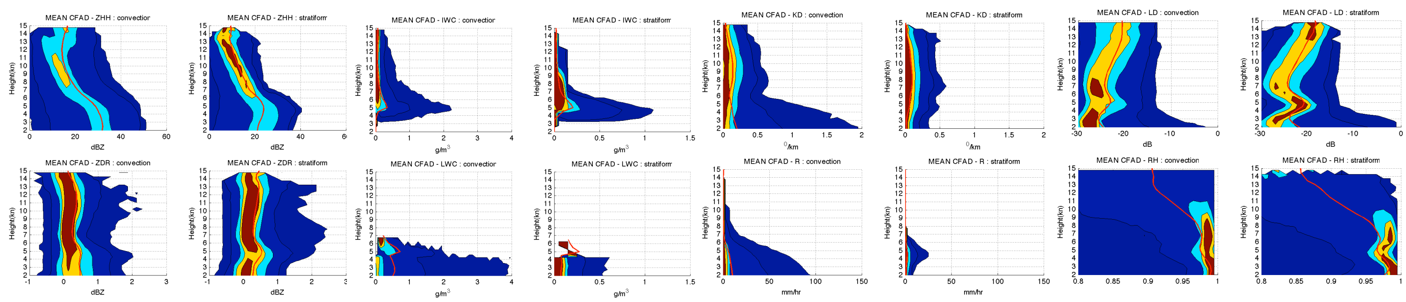

Fig. 10: Same as Fig. 9, but for case 2.

The values of Z_{HH} (Z_{DR}) are about 34 dB (0.72 dB) and 31 dB (0.5 dB) for case 1 and 2, respectively in convective region. The LWC is about 0.51 and 0.49 g/m^3 for case 1 and 2 in convective region and 0.99 and 0.70 g/m^3 for case 1 and 2 near freezing level in convective region. The IWC is about 0.45 and 0.35 g/m^3 for case 1 and 2 near freezing level in convective region. Overall, case 1 contains more LWC and IWC from below freezing to higher level compare to case 2. And both cases are similar in stratiform region in term of Z_{HH}, Z_{DR}, LWC, and IWC

For the K_{DP}, higher values in case 1 compared to case 2 in convective region. Higher rainfall rate in case 1 in convective region. And higher LDR values in freezing layer suggests strong ice-liquid phase mixing. And for RH, lower RH values in freezing layer. Overall, case 1 contains higher rainfall rate and stronger ice-liquid phase mixing (lower RH & higher LDR value near freezing level).

5.Precipitation Efficiency

The values of precipitation efficiency of large scale (LSPE) of both cases are about 50 % in convective region and 10% in stratiform region. The result suggests that only 50 % (10 %) of water vapor from environment been converted into rainfall in convective (stratiform) region. For the cloud microphysical precipitation efficiency (CMPE), both convective and stratiform region of two cases are about 80 ~ 100 %. The result suggests that almost all of the condensate from the condensation of water vapor and deposition of ice, snow and graupel are converted into rainfall.

case		mean area (km²)	mean Rainfall (kg/km²)	mean Vapor Flux (kg/km²)	LSPE	mean Rainfall (kg/km²)	mean $[S_c]$ (kg/km²)	mean $\partial[C]$ (kg/km²)	mean $[CONV_C]$ (kg/km²)	CMPE
14th June 0922 ~ 1200 UTC	con.	2243	1420061	2910324	48.8%	1125842	1305532	-27771	-207462	86.2%
	str.	4184	204273	1711037	11.9%	86641	104468	46688	28861	82.9%
14th June 2030 ~ 2352 UTC	con.	1988	1169720	2692877	43.4%	1106900	1087602	-5685	13612	101.7%
	str.	3799	197018	1740377	11.3%	89532	110456	14450	-6472	81.0%

Table 1: The list of mean rainfall rate, water vapor flux, mean source of cloud condensate, mean cloud water change and convergence of cloud water for case 1 and 2. The corresponding LSPE and CMPE are listed as well.

Further examine the relationship between Z_{HH} - Z_{DR} - LSPE and LWC - Z_{DR} - LSPE (Fig. 11), the higher LSPE is associated with higher Z_{HH} and LWC below freezing level. It's noticeable that given the same Z_{HH} and LWC, the LSPE increases with the increasing of raindrop size (higher Z_{DR}). Indicating the DSD with high concentration of small raindrop has lower LSPE.

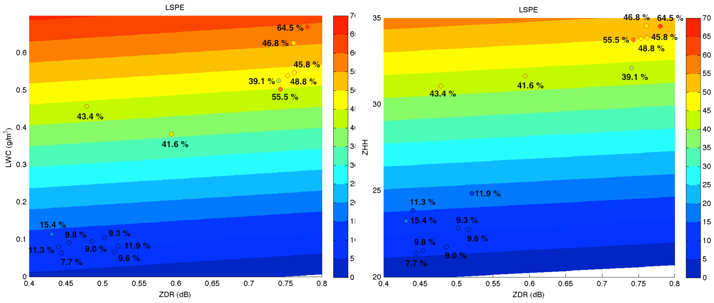

Fig. 11: The relation between Z_{HH}, Z_{DR} and LSPE (left) and LWC, Z_{DR} and LSPE (right). The color shaded represents the first order fitting.

6.Summary

Two convective precipitation of the squall line on June 14, 2008 during TiMREX were examined in terms of kinematic, microphysical field and PE. For kinematic field, the maximum updraft is about 10 m/sec at 10 km MSL, the maximum downdrafts (8 m/sec) locate at the downstream. The Microphysical field, the IWC at convective region reaches about 2.5 g/m^3 and LWC can be higher than 4.0 g/m^3. The ice-water mixing is strong near freezing level at convective region, and the bright-band can be found at most of stratiform region.

Precipitation efficiency: LSPE increases with higher LWC and larger raindrop (higher Z_{DR}).The mean LSPE for this squall line is about 45 % and 10.6 % for convective and stratiform region. And overall averaged LSPE is about 30.9 %. The CMPE is nearly 80 ~ 100 % for convective and stratiform region.

Area	LSPE	CMPE
Convection(31%)	45.3%	96.46%
Stratiform (69 %)	10.6%	129.75%
Total	30.9%	100.10%

Table 2: The mean LSPE and CMPE for convective, stratiform and for overall area.

Reference:
Carey, Lawrence D., Steven A. Rutledge, 2000: The Relationship between Precipitation and Lightning in Tropical Island Convection: A C- Band Polarimetric Radar Study. *Mon. Wea. Rev.*, 128, 2687–2710.
Liou, Y.C., and Y.J. Chang, 2009: A Variational Multiple–Doppler Radar Three-Dimensional Wind Synthesis Method and Its Impacts on Thermodynamic Retrieval. *Mon. Wea. Rev.*, 137, 3992–4010.
Steiner, M., R. A. Houze Jr., and S. E. Yuter, 1995: Climatological characteristics of three-dimensional storm structure from operational radar and rain gauge data. J. Appl. Meteor., 34, 1978–2007.
Sui, Chung-Hsiung, Xiaofan Li, Ming-Jen Yang, Hsiao-Ling Huang, 2005: Estimation of Oceanic Precipitation Efficiency in Cloud Models. *J. Atmos. Sci.*, 62, 4358–4370.
Vivekanandan, J., Guifu Zhang, Edward Brandes, 2004: Polarimetric Radar Estimators Based on a Constrained Gamma Drop Size Distribution Model. *J. Appl. Meteor.*, 43, 217–230.
Vivekanandan, J., S. M. Ellis, R. Oye, D. S. Zrnic, A. V. Ryzhkov, J. Straka, 1999: Cloud Microphysics Retrieval Using S-band Dual-Polarization Radar Measurements. *Bull. Amer. Meteor. Soc.*, 80, 381–388